ORIGINAL PAPER

Molecular modeling of temperature dependence of solubility parameters for amorphous polymers

Xianping Chen · Cadmus Yuan · Cell K. Y. Wong · Guoqi Zhang

Abstract A molecular modeling strategy is proposed to describe the temperature (T) dependence of solubility parameter (δ) for the amorphous polymers which exhibit glass-rubber transition behavior. The commercial forcefield "COMPASS" is used to support the atomistic simulations of the polymer. The temperature dependence behavior of δ for the polymer is modeled by running molecular dynamics (MD) simulation at temperatures ranging from 250 up to 650 K. Comparing the MD predicted δ value at 298 K and the glass transition temperature (T_g) of the polymer determined from δ–T curve with the experimental value confirm the accuracy of our method. The MD modeled relationship between δ and T agrees well with the previous theoretical works. We also observe the specific volume (v), cohesive energy (U_{coh}), cohesive energy density (E_{CED}) and δ shows a similar temperature dependence characteristics and a drastic change around the T_g. Meanwhile, the applications of δ and its temperature dependence property are addressed and discussed.

Keywords Glass transition temperature · Molecular simulation · Solubility parameter

X. Chen · C. K. Y. Wong · G. Zhang
Department of Precision and Microsystem Engineering,
Delft University of Technology,
Mekelweg 2,
2628 CD Delft, the Netherlands

X. Chen · G. Zhang
The Faculty of Mechanical & Electrical Engineering,
Guilin University of Electronic Technology,
541004 Guilin, China

X. Chen (✉) · C. Yuan
Delft Institute of Microsystems and Nanoelectronics (DIMES),
Delft University of Technology,
Feldmannweg 17,
2628 CT Delft, the Netherlands
e-mail: xianping.chen@hotmail.com

C. Yuan
TNO IenT, Materials Technology,
De Rondom 1,
5612 AP Eindhoven, the Netherlands

G. Zhang
Philips Lighting,
Mathildelaan 1,
5611 BD Eindhoven, the Netherlands

Introduction

The solubility parameter, δ, concept provides a numerical estimate of the degree of interaction between materials, and can be a good indication of solubility, particularly for polymers [1–8]. As Bicerano emphasized in his book [8], the utilizations of polymers in many technological and industrial applications are critically dependent on their δ. The δ is often used in industry to predict the compatibility [1], permeation [1, 2], and swelling [2], bulk and solution properties [9–12] of polymers. In sensor applications δ can provide insights to predict the swelling changes of polymers in the presence of volatile chemical compounds [13, 14]. Furthermore, it is useful to optimize processing conditions, as well as select the suitable solvent or the optimum solvents combinations in coatings industry [2]. The δ for a pure compound is defined from Hildebrand-Scatchard solution theory as [3–7]

$$\delta = \sqrt{E_{CED}} \tag{1}$$

The δ is defined as the square root of the E_{CED}. The E_{CED} is the amount of energy needed to completely remove

unit volume of molecules from their neighbors to infinite separation (an ideal gas), which is equal to the molar energy of vaporization ($\Delta H_{vap}-RT$) divided by molar volume (V) [4–6]. Equation 1 can then be converted to

$$\delta = \sqrt{\frac{\Delta H_{vap} - RT}{V}} \qquad (2)$$

where ΔH is the molar enthalpy of vaporization, R is the gas constant, with all physical quantities refering to the same temperature T. The division of the Hildebrand parameter into three component Hansen parameters (dispersion force, polar force, and hydrogen bonding force) can be expressed in terms of the individual solubility parameters δ_d, δ_p and δ_h [6, 8]

$$\delta = \sqrt{\delta_d^2 + \delta_h^2 + \delta_p^2} \qquad (3)$$

where δ_d, δ_h, and δ_p are respectively representing Hansen parameter contribution from dispersion, hydrogen bond, and polar interactions [6, 8].

The δ of polymers is a thermophysical property [12–14], and it shows high dependency to the temperature, T [2, 11–16]. In fact, the T_g of a polymer is closely related to its δ [8, 12, 15, 16]. By considering the T effects on the fractional free volume (v_f) and the enthalpy (H) change, Eqs. 4 and 5 have been proposed to describe the relationship between δ and T respectively above and below T_g for the polymers exhibiting a glass-rubber transition.

For a temperature above Tg, $T \geq T_g$, the polymer is at rubbery state [15, 16]

$$\delta(T)^2 = \left[H_C(T_g)\exp(-4\alpha_l\Delta T) + RT^2(\partial \ln v_f/\partial T)\right]/v_l(T)M \qquad (4)$$

where $H_c(T_g)$ is a molar composite enthalpy at T_g consisting of a conformational and an intermolecular interaction component, α_l is the volume thermal expansion coefficient above T_g, M is the molar mass, $v_l(T)$ is the specific volume above T_g, and ΔT equals the temperature difference with reference to T_g ($\Delta T = T - T_g$). The v equals the reciprocal of its mass density (ρ); molar volume equals the molar mass divided by the mass density (ρ) ($V = M/\rho$). Thus, the molar volume can be expressed as $V = vM$. The molar mass of a polymer is a constant.

For a temperature below T_g, $T \leq T_g$, a polymer at glassy state [15]

$$\delta(T)^2 = \left[H_C(T_g)\exp(-4\alpha_l\Delta T) - M\int_T^{T_g}\Delta C_p(T)/dT\right]/v_s(T)M \qquad (5)$$

where $\Delta C_p(T) = C_{pl}(T) - C_{ps}(T)$, with $C_{pl}(T)$ and $C_{ps}(T)$ being the specific heat capacities at a constant pressure (p)

of the polymer in the liquid and glassy states at T respectively, and $v_s(T)$ is the specific volume below T_g.

Although theoretical works [8, 12, 15, 16] have greatly contributed to the understanding of the relationship between δ and T, a number of fundamental questions remain uncovered, for example, more experimental data on δ at different T are required to support Eqs. 4 and 5. However, determination of δ at different T from experimental methods is time consuming and labor intensive. Moreover, Eqs. 4 and 5 are too complex to be applied practically. The δ can be considered to be linear proportional to T separately in a temperature above and below T_g [15, 16]. Thus, Eqs. 4 and 5 can be are respectively simplified to two linear functions: For $T \leq T_g$, when the polymer is at glassy state (solid phase)

$$\delta(T) = m_s(T - T_g) + \delta_g \qquad (6)$$

where δ_g is the δ at T_g and m_s is the thermal coefficient of δ at glassy state (solid phase); For $T \geq T_g$, when the polymer is at rubbery state

$$\delta(T) = m_l(T - T_g) + \delta_g \qquad (7)$$

where m_l is the thermal coefficient of δ at rubbery state (liquid phase).

Equations 6 and 7 show simple mathematical relations between δ and T. Given the m_s (or m_l) and T_g, δ at a given temperature can be calculated easily from the equations. The two equations and the material constants (m_s, m_l and T_g,) is very important for the physical properties of the polymer. They can provide a fundamental understanding of temperature effects on the bulk and solution properties [1–8, 13, 14, 17] and also help in selecting or designing materials for specific applications. Moreover, they can be utilized in setting protocol for processes related to polymer–solvent interactions [1, 2, 15].

Literature [18–20] shows the possibility in calculating the δ of polymers via MD techniques. Additionally, simulations on bulk systems of moderate size (1000–5000 atoms) using recent systematically-derived "class II" forcefields such as "COMPASS" are capable of making predictions of δ with an accuracy that compares with experiment [21–25]. The forcefield describes approximately the potential energy hypersurface on which the atomic nuclei move. An accurate selection of forcefields is a key in enabling accurate predictions of the molecular interactions and material properties [17–25].

COMPASS is a powerful forcefield that supports atomistic simulations of condensed phase materials [23–25]. It has been parameterized and validated using condensed-phase properties in addition to various *ab initio* and empirical data for molecules in isolation [23, 24]. The forcefield enables accurate and simultaneous prediction of structural, conformational, vibrational, and thermophysical

properties, that exist for organic molecules, inorganic small molecules, and polymers in isolation and in condensed phases, and under a wide range of conditions of temperature and pressure [23–25].

In this investigation, our objective is to model the temperature dependence characteristics of δ for emeraldine based polyaniline (EB–PANI) by using the COMPASS forcefield based MD techniques. The decrease of δ with increasing T for the polymer is plotted by running MD simulations at temperatures ranging from 250 up to 650 K and taking readings for δ at various temperatures. Due to the lack of published δ data at temperature other than 298 K, in order to verify the accuracy of our method, two kind of analysis has been are performed: (i) the δ value at 298 K for EB–PANI is predicted and compared with the literature reported data; (ii) the T_g of the polymer is determined from the δ–T curve and compared with the experimental value. The temperature effects on the physical quantities (v, U_{coh} and E_{CED}) used in the definition of δ are also studied. The applications of the temperature dependence of δ on optimizing processing conditions will be addressed and discussed later in the discussion section.

Computational methodology

The use of atomistic methods to furnish a first principle calculation of E_{CED}, is a desirable tool [18–25]. In atomistic simulations, the cohesive energy, U_{coh}, is defined as the increase in energy per mole of a material if all intermolecular forces are eliminated [18, 19, 25]. The E_{CED} corresponds to the cohesive energy per unit volume. It is a measure of the intermolecular forces within a system, and is estimated via the non-bonded van der Waals and electrostatic (includes hydrogen bond) interactions [18–20, 25, 26]. Equation 2 can be written in the form of:

$$E_{CED} = \left(U_{vdw} + U_Q\right)/vM \qquad (8)$$

where U_{vdw} and U_Q are respectively van der Waals and electrostatic energy [8, 14, 18–20, 25]. Hence, the δ can be formally expressed in terms of

$$\delta = \sqrt{\delta_{vdw}^2 + \delta_Q^2} \qquad (9)$$

where δ_{vdw} and δ_Q are respectively representing the contributions from van der Waals forces and electrostatic interactions and

$$\delta_Q = \sqrt{E_Q} = \sqrt{\frac{U_Q}{vM}} \qquad (10)$$

$$\delta_{vdw} = \sqrt{E_{vdw}} = \sqrt{\frac{U_{vdw}}{vM}} \qquad (11)$$

where E_Q is the electrostatic energy density and E_{vdw} is the van der Waals energy density. Counting hydrogen bonding energy to electrostatic energy results in

$$\delta_Q = \sqrt{\delta_h^2 + \delta_p^2} \qquad (12)$$

In the general case of a gas, liquid, or solid at a constant pressure, p, the volume thermal expansion coefficient, α, is given by

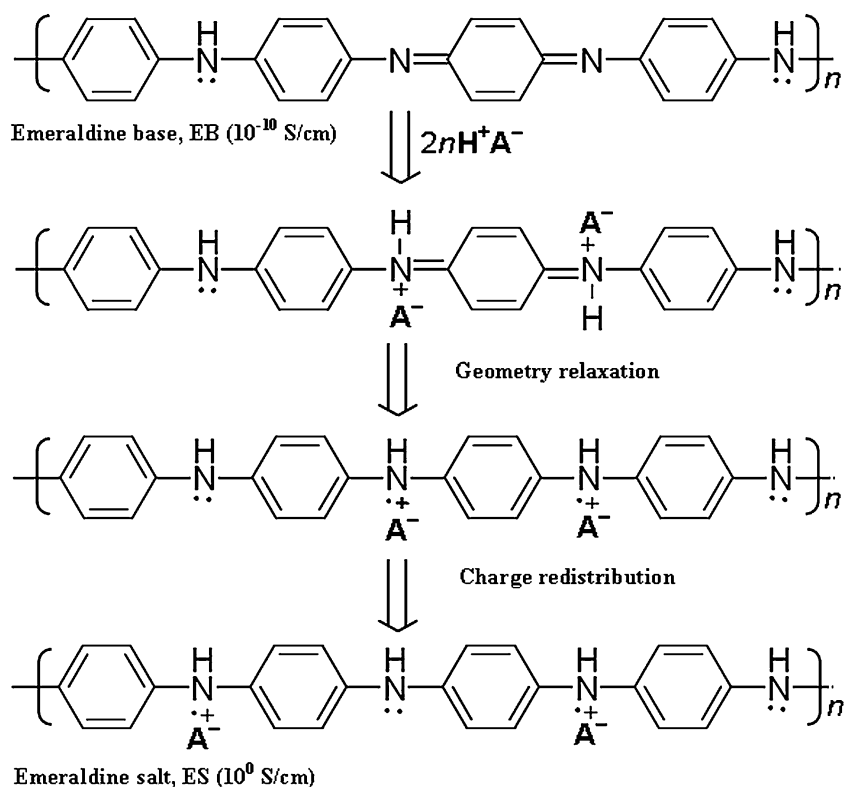$$\alpha = \frac{1}{vM}\left(\frac{\partial v}{\partial T}\right)_p \qquad (13)$$

Since the thermal expansion gradients of α for above and below the T_g are different, and it can be used to predict the T_g of a polymer [25–28]. Applying Eqs. 8–13 to a polymer, the thermal properties of solubility parameter and its related cohesive properties can be investigated and established by MD simulation.

Molecular modeling details

The polymer considered in this work is EB−PANI which consists of equal numbers of reduced (diamine) and oxidized (diimine) units: $[(C_6H_4N)_2(C_6H_4NH)_2]_n$. It is regarded as one of the most useful conducting polymers due to its ease of synthesis, environmental stability and its semi-conductive characteristic upon protonic acid doping (Fig. 1) [25, 29–31]. Structurally, EB–PANI contains benzene rings and amine entity. The cohesive energy contributes from all types of interactions including the polar, the nonpolar (or dispersive), and the specific ones (or hydrogen bonding). The large amounts of benzene rings in the EB–PANI structure enhance the intermolecular interaction among the polymer chains [32–34]. These characteristics inherently make the physical properties of EB–PANI sensitive to temperature. EB−PANI is a good candidate for studying the thermal characteristics of δ and its related cohesive properties.

The molecular simulations are performed by the Forcite Plus module of the commercial software Materials Studio® 5.0 using COMPASS forcefield. Simulation approaches include MM and MD with canonical ensemble (NVT) and isothermal-isobaric ensemble (NPT). All MD simulations are run with a 1.0 fs time step. In all MD simulations, temperature and pressure were controlled by the Berendsen's method using a half-life for decay to the target temperature of 0.1 ps (decay constant) and 0.1 ps for the pressure scaling constant. The non-bonded electrostatic and van der Waals forces are controlled by "atom based" summation and a cutoff value of 15.5 Å is used.

Emeraldine base, EB (10⁻¹⁰ S/cm)

2*n*H⁺A⁻

Geometry relaxation

Charge redistribution

Emeraldine salt, ES (10⁰ S/cm)

Building the amorphous polymer system

The EB−PANI polymer molecule is constructed using the polymer builder based on its stereoisomerism (tacticity) and sequence isomerism (connectivity). The tacticity of the repeat units (Fig. 2a) in the constructed polymer is isotactic. The connectivity of the monomer units (Fig. 2a) is head-to-tail. After geometry optimization, polymer chains are assembled into a three-dimensional (3D) unit cell subject to periodic boundary conditions by an "Amorphous Cell" module. The "Amorphous Cell" module provides a comprehensive set of tools to construct 3D periodic structures of molecular liquids and polymeric systems. The module builds molecules in a cell in a Monte Carlo fashion, by minimizing close contacts between atoms, whilst ensuring a realistic distribution of torsion angles for any given force-field [35]. Using this algorithm, an amorphous polymer structure can be built with realistic conformations, while minimizing the number of close contacts [25, 35].

In order to suppress surface effects while keeping the number of particles in the model to a reasonable size, 3D periodic boundary condition (PBC), in which the system is considered to be surrounded on all sides by replicas of itself (Fig. 2b), has been employed. The length of the cubic unit cell is about 34Å with 3688 atoms (4 polymer chains) (Fig. 2b). Each polymer chain in the amorphous model has 20 monomers and the polymer density is 1.23 g/cm³ [25]. The atomic charges are forcefield assigned [23–25] and

hydrogen bonding interactions have been monitored as illustrated in Fig. 2b.

Geometry optimization and equilibration of polymer system

To create a final structure with realistic density and low-potential-energy characteristics, polymer system is subjected to geometry optimization and an equilibration cycles. The Forcite geometry optimization is employed to refine the geometry of polymer structure until it satisfies a certain criteria with the settings listed in Table 1. Equilibration of polymer system is conducted by an equilibrating protocol which consists of 13 intermediate MD stages (NVT annealings and NPT equilibration) as described in Table 1 [25]. The purpose of an annealing strategy in equilibration is to find the different local minimum energy structures by using the higher temperature periods of each annealing cycle to overcome energy barriers.

Glass-rubber transition of polymer

Once the cell structures have been optimized and equilibrated, NPT–MD simulations over a range of temperature above and below the T_g are employed to model the glass-rubber transition of polymer. Experimentally, the T_g value of EB−PANI range over 460 K interval [(473 K) [33] or (523 K) [34]]. A series of NPT–MD simulations over a temperature range from 250 up to 650 K with an interval of 25 K (each

Fig. 2 **a** Polymer monomer of EB–PANI with COMPASS forcefield assigned atomic charges. **b** Schematic illustration of a cubic unit cell for amorphous EB–PANI. Colors: carbon–gray, hydrogen–white, oxygen–red, nitrogen–blue, and hydrogen bond–red dotted line
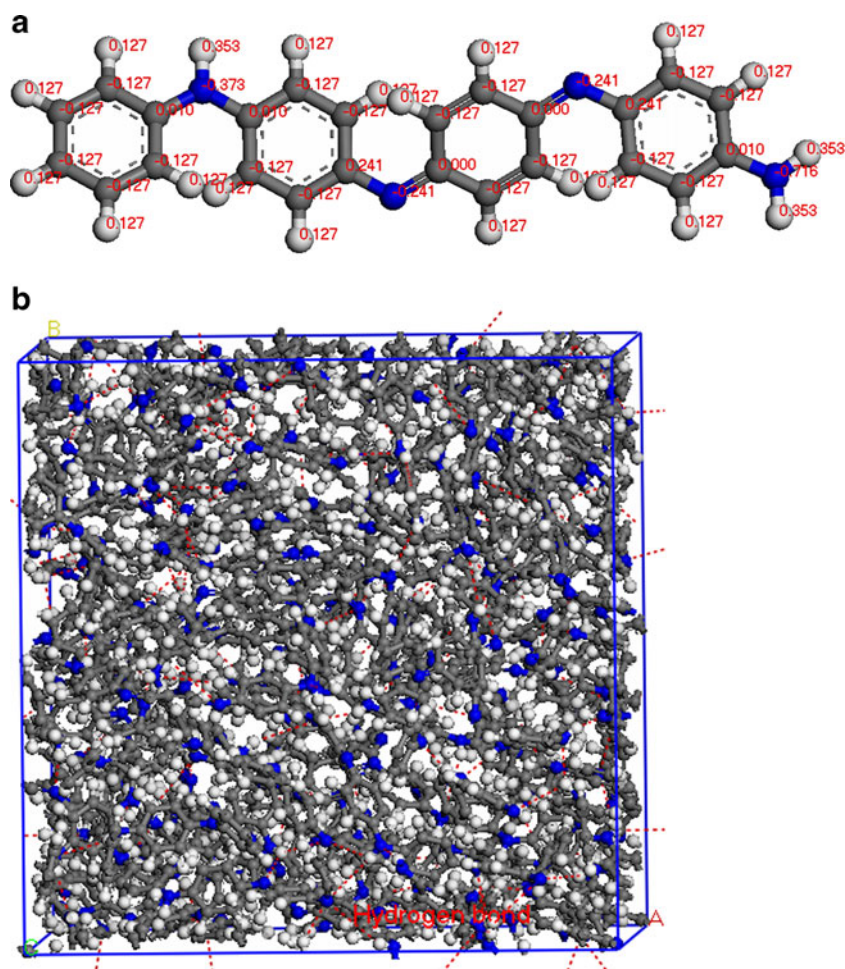
of 500 ps) are carried out for the prediction of T_g. The simulation is continued, with the input of the final state from the previous simulation trajectory. With the simulation trajectory from the NPT–MD simulations, the specific volume, v, and cohesive energy, U_{coh}, at various temperatures is calculated. The δ and its related physical quantities (E_{CED}, E_{vdw}, E_Q), can be calculated by running the Forcite cohesive energy density calculation on the series of structures generated. The three components, van der Waals energy (δ_{vdw}), hydrogen bonding energy (δ_h), and polar interaction (δ_p) contribute to the total solubility parameter, δ, are reported with their associated standard deviation.

Table 1 Settings for geometry optimization and equilibration process of polymer system

Geometry optimization	Equilibration process		
Forcefield: COMPASS	Step	Simulation conditions	Time (ps)
Charges: Forcefield assigned	1	NVT, 750 K	50
Summation method: Ewald for Electrostatic & van der Waals forces	2	A stepwise procedure of NVT of heating and cooling from 600K to 300 K by a step of 50 K	50 ps/step
Algorithm: Smart	3	NVT, 298 K	100
Maximum iterations: Unlimited	4	NPT, 0.1 GPa, 298 K	100
Quality: Ultra-fine;	5, 6	Repeat step 2 and step 3	as above
Energy (kcal mol^{-1}): 2×10^{-5}	7	NPT, 3 GPa, 298 K	100
Force (kcal mol^{-1} Å^{-1}): 0.001	8, 9	Repeat step 2 and step 3	as above
Stress (GPa): 0.001	10	NPT, 0.5 GPa, 298 K	100
Displacement (Å): 1×10^{-5}	11, 12	Repeat step 2 and step 3	as above
External pressure (GPa): 0.0	13	NPT, 0.0001 GPa, 298 K	1,500

Results and discussion

Validation of model in predicting solubility parameter

In order to validate the accuracy, the δ of EB−PANI at 298 K have been predicted and compared with the empirical data. Shacklette and Han determined the total solubility parameters of EB−PANI at 298 K by using empirical measurement and group additive based on Eq. 3. The value of each component is δ_d=17.40 $(J/cm^3)^{1/2}$, δ_h= 10.70 $(J/cm^3)^{1/2}$, and δ_p=8.10 $(J/cm^3)^{1/2}$, which is equivalent to a total solubility parameter of δ=22.2 $(J/cm^3)^{1/2}$ [36–39]. The solubility parameters of EB−PANI at 298 K are estimated in the current MD study as follows: δ_{vdw}=17.94 $(J/cm^3)^{1/2}$, δ_Q=14.07 $(J/cm^3)^{1/2}$, and the total solubility parameter of δ=22.80 $(J/cm^3)^{1/2}$, which are in reasonable agreement with the reported values as listed in Table 2) [36–39]. The agreement between simulation results and empirical data indicates that it is possible to predict the δ at various temperatures by MD.

Temperature dependence of specific volume and cohesive energy

Figure 3a shows that the specific volume as a function of temperature ranging from 250 to 650 K. There is a discontinuity at temperature 498 K, which represents a different thermal expansion in the rubbery and glassy states. Two best-fit lines have been drawn to represent the thermal expansion below and above T_g. The T_g is estimated as the point of intersection (approximately 498 K) between two fit lines. Again, it agrees well with the experimental data which is 473 K [33] and 523 K [34]. In addition to specific volume, the cohesive energy of polymer shows a relatively sudden change at the T_g. To verify this argument, we plot the variation of cohesive energy against the temperature. As illustrated in Fig. 3b, an insignificant discontinuity is observed in the vicinity of T_g. The T_g as determined from the cohesive energy plot is 502 K, which is within the reported range from 473 K [33] to 523 K [34] in the literature. As also indicates from the other groups [27, 28], it demonstrates that T_g can be estimated from change of

Table 2 Comparing the MD simulation predicted solubility parameters with experimental data (T=298 K)

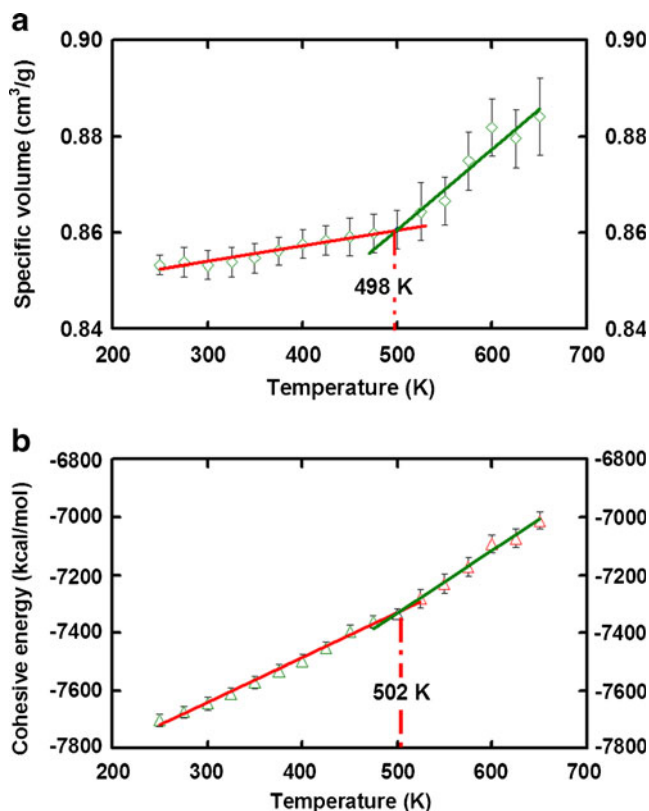| Solubility parameter	Experimental data	MD predicted data
Dispersion (δ_d)	17.40 $(J/cm^3)^{1/2}$	δ_{vdw}=17.94 $(J/cm^3)^{1/2}$
Hydrogen bonding (δ_h)	10.70 $(J/cm^3)^{1/2}$	δ_Q=14.07 $(J/cm^3)^{1/2}$
Polar interaction (δ_p)	8.10 $(J/cm^3)^{1/2}$	
Total solubility parameter (δ)	22.20 $(J/cm^3)^{1/2}$	22.80 $(J/cm^3)^{1/2}$

Fig. 3 Plots of specific volume and cohesive energy against temperature. There is a break in both plots of (**a**) specific volume *vs.* temperature and (**b**) cohesive energy *vs.* temperature. Experimental glass transition temperature of T_g=473 K [33] or 523 K [34]

physical entities along temperature obtained from MD studies.

Temperature effects on the cohesive energy components related to solubility parameters

The thermal properties of total cohesive energy density, van der Waals energy, and electrostatic energy density used in defining δ, have been investigated. Figure 4a−c exhibit the various relationships between different physical entities and temperature (E_{CED} *vs. T*, E_{vdw} *vs. T*, and E_Q *vs. T*). A noticeable break is detected from every plot. The corresponding temperature (493 K in Fig. 4a, 507 K in Fig. 4b, and 486 K in Fig. 4c) of these break are closed to the experimental T_g data [33, 34]. These results indicate the cohesive energy density components versus temperature can also be used to determine T_g. As formulated by Eq. 8, when an amorphous polymer undergoes a phase transition, the specific volume, cohesive energy, and cohesive energy density undergo a drastic change in the vicinity of the glass transition temperature, T_g. The sudden jump at the glass transition temperature in these plots can be regarded as the evidence for Eqs. 4–7 from the previously theoretical works [8, 12, 15, 16].
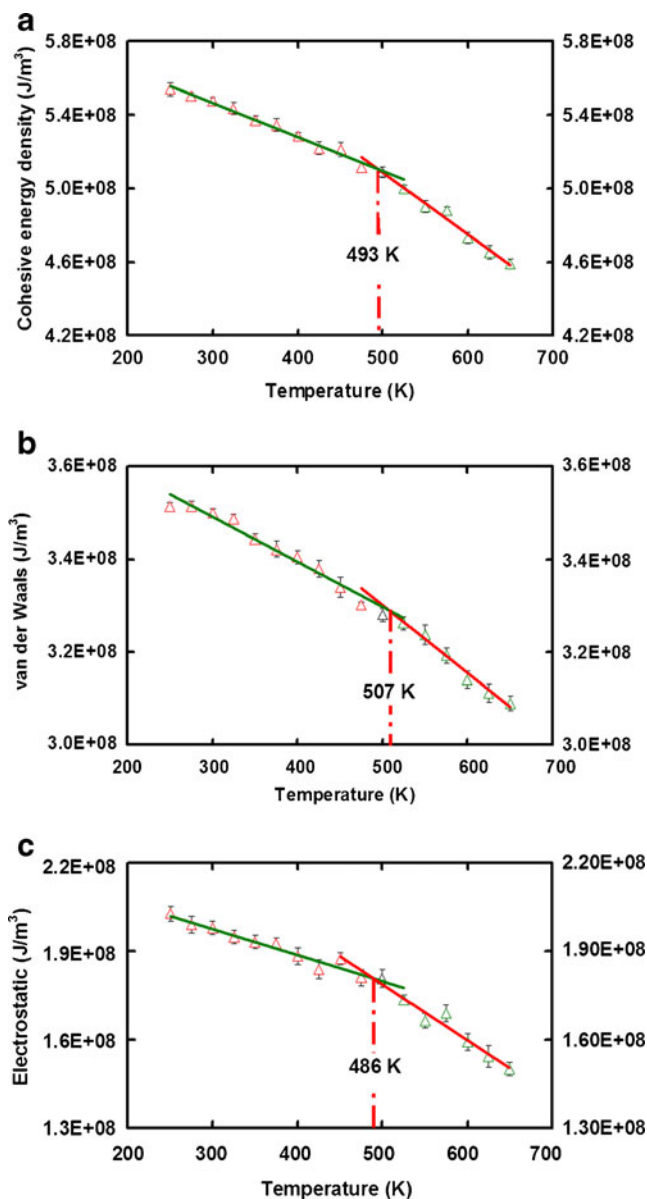
Fig. 4 Plots of cohesive energy density components related to solubility parameter against temperature. There is a discontinuous change in the vicinity of glass transition temperature, T_g, in each plot of (**a**) cohesive energy density (**b**) van der Waals energy density (**c**) electrostatic energy density versus temperature. Experimental glass transition temperature of T_g=473 K [33] or 523 K [34]

Temperature dependence of solubility parameters

Figure 5a shows the variation of the δ of EB−PANI as a function of T ranging from 250 to 650 K. An abrupt change is noticeable at a temperature of 495 K which indicates the occurrence of glass transition. The curve can be split into two linear sections in below and above the breaking point (T_g). In each linear section, the solubility parameter decreases with increasing temperature. The corresponding temperature (495 K) of the breaking point agrees well with the T_g value
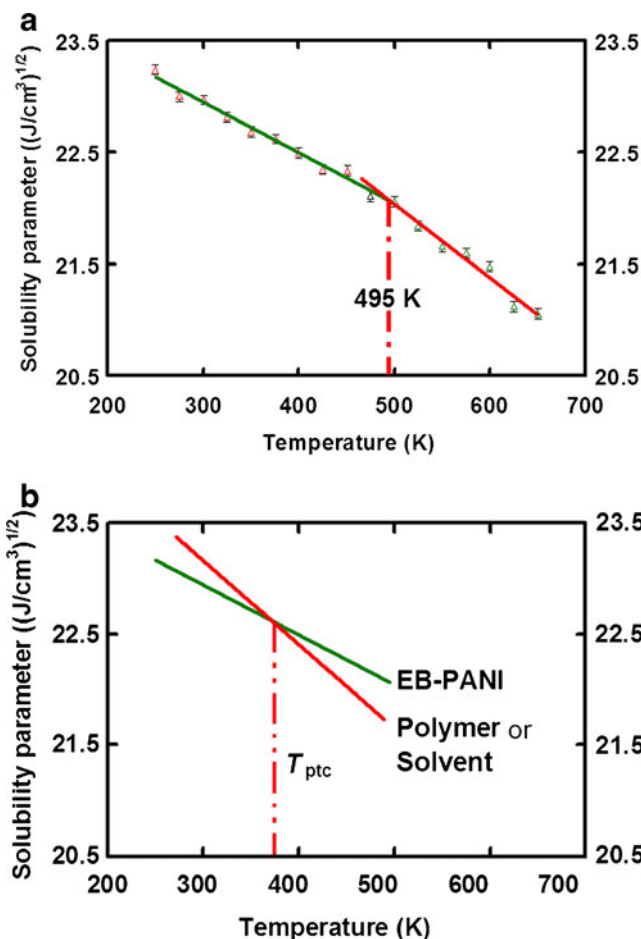

Fig. 5 **a** Plots of solubility parameter against temperature. There is a break at T=495 K in the plot, which indicates the occurrence of glass-rubber transition. Experimental glass transition temperature of T_g= 473 K [33] or 523 K [34]. **b** An example to determine the suitable processing temperature condition (T_{ptc}) by using the δ–T curve. The EB–PANI has the best miscibility (or best solubility) with the target polymer (or solvent) at T_{ptc}

ranges (486 K–507 K) predicted from Fig. 3a–b and Fig. 4a–c, and it is in reasonable agreement with experiment T_g ranges from 473 K [33] to 523 K [34]. Since the T_g is an important characteristic for amorphous polymer, we believe the accuracy in getting T_g from the calculated δ can justify the validation in estimating the δ with MD method.

In applying Eqs. 6 and 7 to the current study, the thermal coefficient of solubility parameter at glassy state (m_s) or liquid state (m_l) and the solubility parameter at glass transition temperature (δ_g) are calculated as:For $T \leq T_g$, the polymer at glassy state

$$\delta(T) = -0.0045(T - T_g) + 22.07 \tag{14}$$

where the thermal coefficient of solubility parameter at solid phase m_s=−0.0045 ((J/cm³)$^{1/2}$ T^{-1}) and the solubility parameter at T_g, δ_g = 22.07((J/cm³)$^{1/2}$.

For $T \geq T_g$, the polymer at glassy state

$$\delta(T) = -0.0066(T - T_g) + 22.07 \qquad (15)$$

where the thermal coefficient of solubility parameter at liquid phase $m_1 = -0.0066$ $((\text{J/cm}^3)^{1/2} T^{-1})$. Equation 14 and Eq. 15 are useful for EB−PANI in the technical and industrial applications. For instance, it can be used to select a second polymer in formulating a polymer composite; incorporating a second component into conducting polymer film is one of the most important methods to develop new sensors [13, 14]. In comparison with modification of molecular structure of conducting polymers, the advantage of this technique is that it can avoid complicated chemical syntheses. Using Eq. 14, we can determine the miscibility of two polymers and the suitable processing temperature condition (T_{ptc}) in fabrication as illustrated in Fig. 5b. In another scenario, the equations can help in the optimization of processing conditions, as well as selecting appropriate solvents or predicting the suitable temperature (see Fig. 5b) for combinations in coatings industry [2].

Conclusions

The molecular modeling methodology, which is capable of investigating the temperature dependence characteristics of δ of amorphous polymer, has been formulated. The temperature effects on δ are studied by running MD simulations at various temperatures. From the δ–T curve, the glassy phase and the rubbery phase are clearly seen. The MD predicted results over the significant range (from 250 up to 650 K) of temperatures are conveniently fitted to the two linear equations (Eqs. 5 and 6) of the form. Comparisons with experimental data confirm the validity of our method. The δ, v, U_{coh}, and E_{CED} show a similar temperature dependence characteristics and a drastic change around the T_g. Thus, the temperature dependence of δ and its related cohesive properties (v, U_{coh}, and E_{CED}) may be utilized in determining T_g of a polymer which has the glass-rubber transition. Furthermore, the applications of the temperature dependence characteristics of δ have been addressed and discussed.

References

1. Inzelt G (2008) Conducting polymers a new era in electrochemistry. Springer, Berlin
2. Shirsat MD, Bangar MA, Deshusses MA, Myung NV, Mulchandani A (2009) Polyaniline nanowires-gold nanoparticles hybrid network based chemiresistive hydrogen sulfide sensor. Appl Phys Lett 94 (083502):1–3
3. Scatchard G (1931) Equilibria in non-electrolyte solutions in relation to the vapor pressures and densities of the components. Chem Rev 8:321–333
4. Hildebrand JH (1916) Solubility. J Am Chem Soc 38:1452–1473
5. Hildebrand JH (1919) Solubility III. Relative values of internal pressures and their practical application. J Am Chem Soc 41:1067–1080
6. Barton AFM (1975) Solubility parameters. Chem Rev 75:731–753
7. Hildebrand JH, Prausnitz JM, Scott RL (1970) Regular and related solutions: The solubility of gases, liquids, and solids. Reinhold, New York
8. Bicerano J (2002) Prediction of polymer properties. Dekker, New York
9. Gardon JL (1963) Relationship between cohesive energy densities of polymers and Zisman's critical surface tensions. J Phys Chem 67:1935–1936
10. Girifalco LA, Good RJ (1957) A theory for the estimation of surface and interfacial energies. I. derivation and application to interfacial tension. J Phys Chem 61:904–909
11. Hildebrand JH, Scott RL (1964) The solubility of non-electrolytes. Dover Publications, New York
12. Hayes RA (1961) The relationship between glass temperature, molar cohesion, and polymer structure. J Appl Polym Sci 5:318–321
13. Nanto N, Dougami N, Mukai T, Habara M, Kusano E, Kinbara A, Ogawa T, Oyabu T (2000) A smart gas sensor using polymer-film-coated quartz resonator microbalance. Sens Actuators B 66:16–18
14. Shevade AV, Ryan MA, Homer ML, Manfreda AM, Zhou H, Manatt KS (2003) Molecular modeling of polymer composite–analyte interactions in electronic nose sensors. Sens Actuators B 93:84–91
15. Chee KK (2005) Temperature dependence of solubility parameters of polymers. Malaysian J Chem 7:57–61
16. Tanaka N (1992) Prediction of solubility parameter from thermal transition behaviour in polymers. Polym 33:623–626
17. Charles M, Hansen, Just L (2001) Prediction of environmental stress cracking in plastics with Hansen solubility parameters. Ind Eng Chem Res 40:21–25
18. Patrick J, Marsac, Sheri L, Shamblin, Lynne S, Taylor L (2006) Theoretical and practical approaches for prediction of drug–polymer miscibility and solubility. Pharm Res 23:2417–2426
19. Belmares M, Blanco LM, Goddard WA III, Ross RB, Caldwell G, Chou SH, Pham J, Olofson PM, Thomas C (2004) Hildebrand and Hansen solubility parameters from molecular dynamics with applications to electronic nose polymer sensors. J Comput Chem 25:1814–1826
20. Tantishaiyakul V, Worakul N, Wongpoowarak W (2006) Prediction of solubility parameters using partial least square regression. Int J Pharm 325:8–14
21. Sun H, Rigby D (1997) Polysiloxanes: *ab initio* forcefield and structural, conformational and thermophysical properties. Spectrochim Acta Part A 53:1301–1323
22. Rigby D, Sun H, Eichinger BE (1998) Computer simulations of poly(ethylene oxides): Forcefield, PVT diagram and cyclization behavior. Polym Int 44:311–330

23. Sun H, Ren P, Fried JR (1998) The COMPASS forcefield: parameterization and validation for polyphosphazenes. Comput Theor Polym Sci 8:229–246
24. Sun H (1998) COMPASS: an *ab initio* forcefield optimized for condensed-phase application-overview with details on alkane and benzene compounds. J Phys Chem B 102:7338–7364
25. Chen XP, Yuan CA, Wong CKL, Zhang GQ (2011) Validation of forcefields in predicting the physical and thermophysical properties of emeraldine base polyaniline. Mol Simulat 37:990–996
26. Barton AFM (1983) Handbook of solubility parameters and other cohesion parameters. CRC Press, Boca Raton
27. Wu CF, Xu EJ (2007) Atomistic molecular simulations of structure and dynamics of crosslinked epoxy resin. Polym 48:5802–5812
28. Fried JR, Li B (2001) Atomistic simulation of the glass transition of di-substituted polysilanes. Comput Theor Polym Sci 11:273–281
29. Chiang JC, MacDiarmid AG (1986) Polyaniline: Protonic acid doping of the emeraldine form to the metallic regime. Synth Met 13:193–205
30. MacDiarmid AG (2001) Nobel Lecture: "Synthetic metals": a novel role for organic polymers. Rev Mod Phys 73:701–712
31. MacDiarmid AG (2001) Synthetic metals: a novel role for organic polymers. Synth Met 125:11–22
32. Cowie JMG, Arrighi V (2007) Polymers: chemistry and physics of modern materials. CRC, Boca Raton
33. Pellegrino J, Radebaugh R (1996) Gas sorption in polyaniline. 1. emeraldine base. Mattes Macromol 29:4985–4991
34. Wei Y, Jang GW, Hsueh KF, Sherr EM, MacDiarmid AG, Epstein AJ (1992) Thermal transitions and mechanical properties of films of chemically prepared polyaniline. Polym 33:314–322
35. Theodorou DN, Suter UW (1985) Shape of unperturbed linear polymers: polypropylene. Macromolecules 18:1206–1214
36. Shacklette L, Han C (1994) Solubility and dispersion characteristics of polyaniline. Mat Res Soc: Symp Proc 328:157–166
37. Gregory RV, Jain R (1995) Solubility and rheological characterization of polyaniline base in N-methyl-2-pyrrolidinone and N, N′-dimethylpropylene urea. Synth Met 74:263–266
38. Skotheim TA, Elsenbaumer RL, Reynolds JR (1998) Handbook of conducting polymers. Dekker, New York
39. van Krevelen DW (1990) Properties of polymers. Elsevier, Amsterdam